This article has been accepted for publication in a future issue of this journal, but has not been fully edited. Content may change prior to final publication. Citation information: DOI 10.1109/TIE.2019.2956391, IEEE Transactions on Industrial Electronics



# Application of Analytic Signal and Smooth Interpolation in Pulse Width Modulation for Conventional Matrix Converters

Pawel Szczepankowski, *Member, IEEE*, Patrick Wheeler, *Senior Member, IEEE*, Tomasz Bajdecki

***Abstract*—The paper proposes an alternative and novel approach to the PWM duty cycles computation for Conventional Matrix Converters (CMC) fed by balanced, unbalanced or non–sinusoidal AC voltage sources. The presented solution simplifies the prototyping of direct modulation algorithms. PWM duty cycles are calculated faster by the smooth interpolation technique, using only vector coordinates, without trigonometric functions and angles. Both input voltages and output reference voltages are expressed by analytic signals in the proposed direct modulation. Input voltages are represented by the rotating vector collection in the two–dimensional Cartesian coordinate system. All reference output voltages are located inside the triangular surface, named here as the voltage synthesis field, formed by these rotating vectors. A certain degree of reference signals placement freedom allows to maximize the voltage transfer ratio to $0.866$ with less switching compared to the Optimum–Venturini direct method. The proposed solution was verified by simulations and experiments for CMC$3 \times k$. The comparison with the Optimum–Venturini modulation is included. The proposed PWM duty cycle computation approach can also be applied to multiphase CMC converters for any number of inputs as well as outputs.**

***Index Terms*—AC-AC converters, matrix converters, pulse width modulation.**

## NOMENCLATURE

| | |
|---|---|
| $j$ | $\sqrt{-1}$. |
| x | Real part subscript of complex number. |
| y | Imaginary part subscript of complex number. |
| i | Subscript corresponding to input of CMC. |
| o | Subscript corresponding to output of CMC. |
| $k$ | Number of outputs. |
| $T$ | Transposition of the matrix. |
| $\mathbf{v}_\mathrm{i}$ | Measured input voltages $[v_{\mathrm{i}1}, v_{\mathrm{i}2}, v_{\mathrm{i}3}]^T$. |
| $\mathbf{v}_\mathrm{o}$ | Average output voltages $[v_{\mathrm{o}1}, v_{\mathrm{o}2}, ..., v_{\mathrm{o}k}]^T$. |
| $\overline{\mathbf{v}}_\mathrm{i}$ | $= \mathbf{v}_{\mathrm{ix}} + j \cdot \mathbf{v}_{\mathrm{iy}}$ Analytic form of input voltage. |
| $\overline{\mathbf{v}}_\mathrm{o}$ | $= \mathbf{v}_{\mathrm{ox}} + j \cdot \mathbf{v}_{\mathrm{oy}}$ Analytic form of output voltage. |
| $\mathbf{i}_\mathrm{i}$ | Average input currents $[i_{\mathrm{i}1}, i_{\mathrm{i}2}, i_{\mathrm{i}3}]^T$. |
| $\mathbf{i}_\mathrm{o}$ | Measured output currents $[i_{\mathrm{o}1}, i_{\mathrm{o}2}, ..., i_{\mathrm{o}k}]^T$. |

Manuscript received May 22, 2019; revised August 21, 2019; accepted November 13, 2019. This work was supported by the LINTE$^2$ Laboratory, Gdansk University of Technology.

Pawel Szczepankowski, Gdansk University of Technology, POLAND, (e-mail: pawel.szczepankowski@pg.edu.pl)

Pat Wheeler, University of Nottingham, UK, (e-mail: pat.wheeler@nottingham.ac.uk)

Tomasz Bajdecki, Institute of Power Engineering, Gdansk Division, POLAND, (e-mail: t.bajdecki@ien.gda.pl)

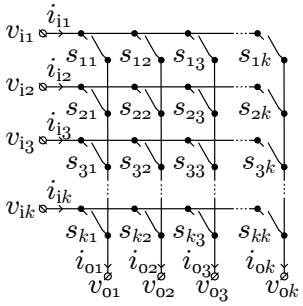


Fig. 1: Conventional $k$-phase Matrix Converter.

| | |
|---|---|
| $\mathbf{d}_n$ | PWM duty cycle matrix for $n$ output $[d_{1n}, d_{2n}, d_{3n}]^T$. |
| $\mathbf{D}$ | Complete PWM duty cycle matrix for all switches. |
| $\phi_\mathrm{i}$ | Input displacement angle. |
| $\omega_\mathrm{i}$ | $= 2\pi f_\mathrm{i}$, where $f_\mathrm{i}$ is the source frequency. |
| $\omega_\mathrm{o}$ | $= 2\pi f_\mathrm{o}$, where $f_\mathrm{o}$ is the load frequency. |
| $q$ | $= V_\mathrm{o}/V_\mathrm{i}$ Voltage transfer ratio. |
| $q_{\max}$ | Maximum value of voltage transfer ratio. |
| $\Delta_{[1,2,3]}$ | Area of triangle $\Delta$ with vertices 1, 2, and 3. |

## I. INTRODUCTION

THE CMC, shown in Fig. 1, is an AC–AC power converter which generates the load voltage with arbitrary amplitude and frequency with unity input power factor operation and sinusoidal input and output currents [1], [2]. Many PWM modulation strategies have been widely reported in literature, mainly as the direct control by Venturini approach [3]–[5], scalar control realized according to Roy method [6], carrier based modulation method (CBPWM) and the Space Vector Modulation (SVM) [7], [8]. In addition to the numerous applications in a multiphase electric drive, due to their advantages over classic solutions [9]–[12], matrix converters also find use in an energy conditioning solutions [13], [14]. Research on matrix converters has resulted in multilevel and indirect topologies [15], [16]. However, this topology is still interesting in terms of both in the application and prototype design [17], [18].

Many PWM modulation algorithms reported in literature are usually focused on the three inputs with an assumption of sinusoidal input waveforms. Although several articles provide modulation schemes under unbalanced sources or abnormal input conditions, the studies concern the CMC$3 \times 3$ case [19]–[21], while the CMC$m \times n$ case seems not be much explored.

As presented in [22] the $m \times n$ topology can also be used in multiphase wind energy generation with a direct matrix converter using a general approach introduced in [23]. Due to the requirements of multiphase machines and converters, the classic Venturini's technique has been adopted and extended in [23] using advanced trigonometrical approach. Modulating signals have been elaborated and proposed for a number of inputs greater than three, whereas the PWM duty cycle computation formula has not been proposed so far. A similar solution developed using heuristic methods has been presented in [24], where research results have been only demonstrated for three inputs, under the assumption of the balanced voltage source. A new interesting idea of a direct modulation is also proposed in [25], where detailed mathematical treatment, based on the power balance equations, is described. This modulation approach only addresses the CMC$3 \times 3$ converter.

To conclude, the elaboration of the PWM duty cycle computing formula for the direct method of modulation is a challenging task due to different numbers of inputs and outputs – in particular when the number of inputs is greater than the number of outputs. A second important issue concerning modulation algorithms is to maintain the good quality of load currents during abnormal input voltage conditions. Thus, the PWM duty cycle computing issue becomes more and more complicated for multiphase topologies. The aims of this paper are as follows:

- to find a general, understandable and easy to apply the description of the direct AC voltages synthesis for symmetrical three–phase power supply, that is not limited to sinusoidal voltages and allows to reach the maximum voltage transfer ratio and adjusting the power angle at the input of the system for any number of the output voltages.
- to formulate assumptions of the load voltage synthesis in systems with any number of the output phases and arbitrarily selected sets of input voltages.
- to maintain the sinusoidal current at the output of CMC with voltage synthesis based on unbalanced or nonsinusoidal AC sources.

The second important aspect is the time reduction of executing the program instructions, as well as the simplification of the calculation scheme. The Gallium Nitride (GaN) and Silicon Carbide (SiC) semiconductors offer fundamental advantages over silicon solutions, in particular, the higher critical electrical field and smaller capacitances compared to silicon switches [26]–[31]. The switching frequency of these power semiconductors can be very high compared to the silicon counterparts, which makes these devices great for high–frequency application [32], [33]. Elimination of the trigonometry and angles from the algorithm, due to their computing time, allows to implement the proposed CMC control in FPGA digital structures using the standard function blocks.

The paper proposes a solution of the direct AC–AC conversion also for non–sinusoidal and deformed sources for any number of converter inputs and outputs. The smooth interpolation method described in section V was used for the implementation of the voltage synthesis for a given number of output voltages based on a selected dynamically number of inputs.

Section II contains a brief introduction into the analytic signals and the voltage synthesis field concepts. The proposed approach of fast PWM duty cycle computing for CMC with three inputs is explained in section III. The method of PWM duty cycle computation is demonstrated in section IV, where a Direct Analytic Vector – PWM (DAV–PWM) for CMC with $k$–outputs is presented. Section V discusses the assignments of Wachspress's smooth interpolation method for generalization of the AC–AC voltage synthesis. Simulation results are presented in section VI, while experimental research, including the comparative results, are placed in the next section.

## II. Analytic Signal concept

Signal $z(t)$ which has no negative–frequency components is called an analytic signal [34], [35] and in continuous time can be represented as

$$z(t) = \frac{1}{2\pi} \int_0^{\infty} Z(\omega) e^{j\omega t} d\omega \tag{1}$$

where $Z(\omega)$ is the complex coefficient which sets the amplitude $|\vec{z}|$ and phase $\varphi(t)$, shown in Fig. 2(a), of the positive–frequency complex sinusoid $\exp(j\omega t)$ at frequency $\omega$. The sampled input voltages, which are usually the pure three sinusoids

$$\begin{aligned} v_{\mathrm{i1x}} &= V \cos(\omega_{\mathrm{i}} t) \\ v_{\mathrm{i2x}} &= V \cos(\omega_{\mathrm{i}} t + 2\pi/3) \\ v_{\mathrm{i3x}} &= V \cos(\omega_{\mathrm{i}} t - 2\pi/3) \end{aligned} \tag{2}$$

by generating a phase–quadrature components

$$\begin{aligned} v_{\mathrm{i1y}} &= V \sin(\omega_{\mathrm{i}} t) \\ v_{\mathrm{i2y}} &= V \sin(\omega_{\mathrm{i}} t + 2\pi/3) \\ v_{\mathrm{i3y}} &= V \sin(\omega_{\mathrm{i}} t - 2\pi/3) \end{aligned} \tag{3}$$

can be converted to a set of positive–frequency complex expressions

$$\begin{aligned} \bar{v}_{\mathrm{i1}} &= V e^{j\omega_{\mathrm{i}} t} \\ \bar{v}_{\mathrm{i2}} &= V e^{j(\omega_{\mathrm{i}} t + 2\pi/3)} \\ \bar{v}_{\mathrm{i3}} &= V e^{j(\omega_{\mathrm{i}} t - 2\pi/3)} \end{aligned} \tag{4}$$

by a well known quarter–cycle time shift method or using the Clarke transform–based formula as follows

$$\begin{bmatrix} v_{\mathrm{i1x}} & v_{\mathrm{i1y}} \\ v_{\mathrm{i2x}} & v_{\mathrm{i2y}} \\ v_{\mathrm{i3x}} & v_{\mathrm{i3y}} \end{bmatrix} = \begin{bmatrix} v_{\mathrm{i1x}} & v_{\mathrm{i2x}} & v_{\mathrm{i3x}} \\ v_{\mathrm{i2x}} & v_{\mathrm{i3x}} & v_{\mathrm{i1x}} \\ v_{\mathrm{i3x}} & v_{\mathrm{i1x}} & v_{\mathrm{i2x}} \end{bmatrix} \begin{bmatrix} 1 & 0 \\ 0 & 1/\sqrt{3} \\ 0 & -1/\sqrt{3} \end{bmatrix} \tag{5}$$

The positive complex expression from (4) can be represented by three rotating vectors in $xy$ two–dimensional coordinate system, as shown in Fig. 2(b). In most practical cases, the quality of the grid supply voltage is proper and the calculation of quadrature components is reduced to the equation (5), then the proposed algorithm takes a simple effective form. The calculation of analytical signals for AC unbalanced and distorted voltages requires the use of advanced operations. This is however not the disadvantage of the proposed approach because frequency analysis is widely implemented and supported in DSP processors and FPGA devices. If high precision of output voltage generation is needed, the accurate calculation of vectors coordinates requires the Hilbert Transform Filter

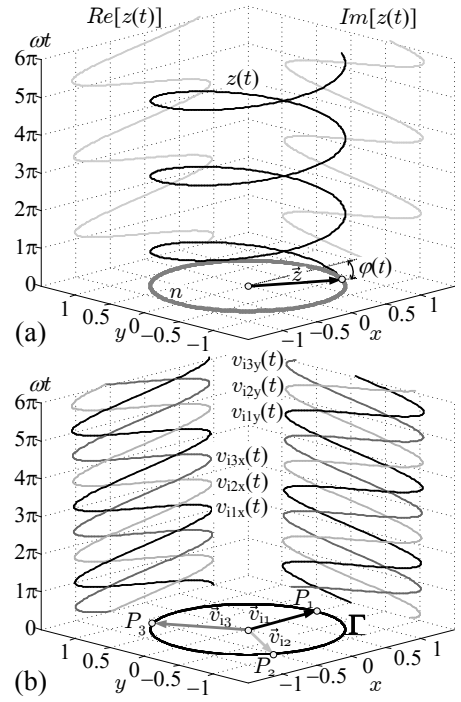


Fig. 2: Geometrical interpretation of analytic signal: (a) theoretical trajectory $\Gamma$ of signal $z(t)$, (b) three pure sinusoids representation by rotating vectors in $xy$ reference frame.

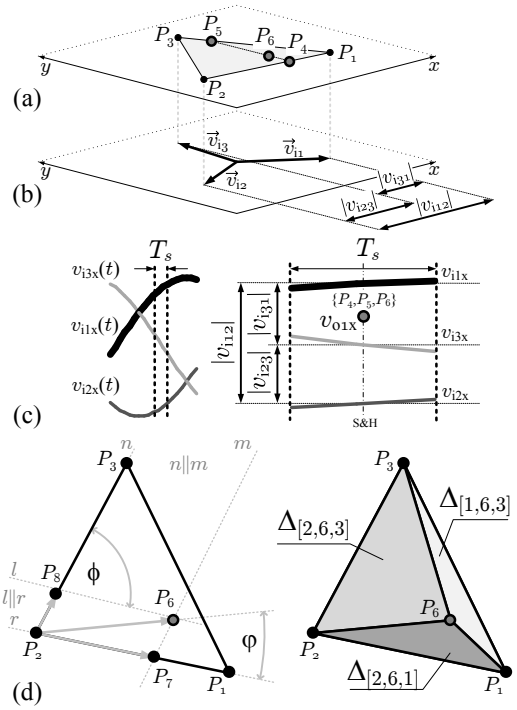


Fig. 3: Presentation of the main geometric relationships between the input and output voltages: (a) the voltage synthesis field, (b) three input rotating vectors, (c) the $real$ value of the reference output voltage $v_{\mathrm{o1x}}$ within sampling interval $T_S$, (d) vectors arrangement to perform general algebraic construction of PWM duty cycles computation.

[36] or other operation based on Fast Fourier Transform (FFT) [37]. The calculation can be limited to several dominant harmonics, thus the Discrete Fourier Transform (DFT) based approach, such as moving–window DFT, may be applied [38].

Each AC input voltage waveform can be represented by an analytic signal and samples of these input voltages are transformed into points with coordinates $xy$. These points – minimum three selected – are vertices of the convex polygon, which is the voltage synthesis field. A similar proposal was introduced in [39] as the Duty Cycle Space Vectors concept, in which the synthesis field is presented only as of the stationary equilateral triangle, which does not rotate and cannot express abnormal voltage conditions such as unbalance and higher–order harmonics. For three–phase balanced sources, even if they are not sinusoidal, the synthesis field can be easily constructed using (5). For symmetric and balanced multi–phase voltage sources the algebraic construction of the voltage synthesis field is rather intuitive. If the input voltages are arbitrary and do not create symmetric voltage systems or contain higher harmonics, a precise AC–AC conversion requires special signal processing techniques, as reported earlier.

Input voltages can be expressed by analytic signals, which are represented by the Hilbert pairs – the $real$ (which is physically measurable), and the $imaginary$ values. There are exactly three pairs, represented by points $P_1$, $P_2$, and $P_3$ shown in Fig. 3(a), for the three–phase AC voltage source. Moreover, as presented in Fig. 3(b), the distances between the $real$ coordinates of these points are equal to the instantaneous line–to–line voltages. The reference output voltages can be also represented by the $real$ and $imaginary$ values and only the $real$ coordinate $v_{\mathrm{o1x}}$, shown in Fig. 3(c), directly influences the output currents. Theoretically, the value of the imaginary components can be arbitrary. However, all instantaneous output voltages, due to the physical restriction, are limited by the input voltages envelope. This limitation can be expressed graphically by the triangle named the voltage synthesis field as proposed previously.

## III. PWM Duty Cycle Computation for CMC with three inputs

A mathematical expression for computing the PWM duty cycles can be constructed in an explicit algebraic form based on coordinates of the triangle vertices [40]. These coordinates are presented in the two–dimensional Cartesian reference frame. Considering the vector arrangement illustrated in Fig. 3(a), points $P_4$ and $P_5$ represent two basic cases, while point $P_6$ – with the same $x$ coordinate – designates the general output vector position $\vec{v}_{\mathrm{o1}}$ in the voltage synthesis field. The following proportions based on the sine rule applied to the geometry as in Fig. 3(d) can be formulated

$$\frac{|P_2P_6|}{\sin(\pi-\phi)} = \frac{|P_2P_8|}{\sin(\varphi)} = \frac{|P_2P_7|}{\sin(\phi-\varphi)} \tag{6}$$

Duty cycles $d_1$ and $d_3$, which correspond to points $P_1$ and $P_3$ respectively, can be calculated as a ratio of the absolute value

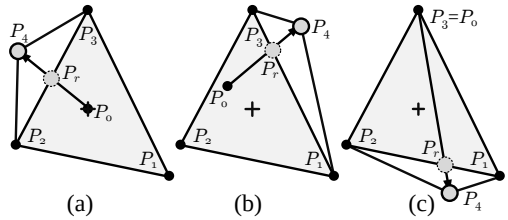


Fig. 4: The point $P_4$ positions outside the synthesis field: (a) the vector origin is located at the point (0,0), (b) the origin has arbitrary interior location, (c) the origin represented by $P_0$ overlaps point $P_3$.

of the appropriate vector products as expressed below

$$d_1 = \frac{|P_2P_7|}{|P_2P_1|} = \frac{|P_2P_6|}{|P_2P_1|}\frac{\sin(\phi-\varphi)}{\sin(\phi)}\cdot\frac{|P_2P_3|}{|P_2P_3|} = \frac{\left|\overrightarrow{P_2P_6}\times\overrightarrow{P_2P_3}\right|}{\left|\overrightarrow{P_2P_1}\times\overrightarrow{P_2P_3}\right|} \tag{7}$$

$$d_3 = \frac{|P_2P_8|}{|P_2P_3|} = \frac{|P_2P_6|}{|P_2P_3|}\frac{\sin(\varphi)}{\sin(\phi)}\cdot\frac{|P_2P_1|}{|P_2P_1|} = \frac{\left|\overrightarrow{P_2P_6}\times\overrightarrow{P_2P_1}\right|}{\left|\overrightarrow{P_2P_3}\times\overrightarrow{P_2P_1}\right|} \tag{8}$$

Note, that the magnitude of the cross product of two vectors is the area of the parallelogram with the two vectors as adjacent sides. Thus, equations (7) and (8) can be transformed finally to expression

$$d_1 = \xi\cdot\left|\det\begin{bmatrix} v_{\mathrm{i2x}}-v_{\mathrm{o1x}} & v_{\mathrm{i2y}}-v_{\mathrm{o1y}} \\ v_{\mathrm{i3x}}-v_{\mathrm{o1x}} & v_{\mathrm{i3y}}-v_{\mathrm{o1y}}\end{bmatrix}\right| = \frac{\Delta_{[2,6,3]}}{\Delta_{[1,2,3]}} \tag{9}$$

$$d_3 = \xi\cdot\left|\det\begin{bmatrix} v_{\mathrm{i1x}}-v_{\mathrm{o1x}} & v_{\mathrm{i1y}}-v_{\mathrm{o1y}} \\ v_{\mathrm{i2x}}-v_{\mathrm{o1x}} & v_{\mathrm{i2y}}-v_{\mathrm{o1y}}\end{bmatrix}\right| = \frac{\Delta_{[2,6,1]}}{\Delta_{[1,2,3]}} \tag{10}$$

where $\det$ means the determinant of the matrix $2\times 2$, and

$$\xi = \left|\det\begin{bmatrix} v_{\mathrm{i2x}}-v_{\mathrm{i1x}} & v_{\mathrm{i2y}}-v_{\mathrm{i1y}} \\ v_{\mathrm{i3x}}-v_{\mathrm{i1x}} & v_{\mathrm{i3y}}-v_{\mathrm{i1y}}\end{bmatrix}\right|^{-1} \tag{11}$$

Thus, any angles or trigonometric functions do not need to be ever evaluated. If the reference vector $\overrightarrow{P_0P_4}$ lies outside the synthesis field, as in Fig. 4(a)–(c), the length of this vector can be shortened in respect to its original point $P_0$ and direction by the following factor

$$\gamma_{(\mathrm{a})} = \frac{|P_0P_r|}{|P_0P_r|+|P_rP_4|} = \frac{\Delta_{[0,2,3]}}{\Delta_{[0,2,3]}+\Delta_{[2,3,4]}} \tag{12}$$

for the case (a), and in the analogous way for cases (b) and (c). Each reference output voltage sample can be also presented as the pair of two coordinates. Only the $real$ part, which corresponds to $x$ coordinate, determines the peak–to–peak output line–to–line voltage, while the $imaginary$ part can be modified to obtain certain features of the PWM modulation, such as the control of the input displacement angle $\phi_{\mathrm{i}}$. Modifications cannot move any reference point outside the synthesis field [41]. Changes in the position of the pair representing the output voltage in the synthesis field can be expressed by $\Gamma$ trajectory shape, as shown in Fig. 2(b), where the circular trajectory is presented.

The main purpose of modifying the $real$ part is increasing the range of linear modulation. For the basic circular trajectory

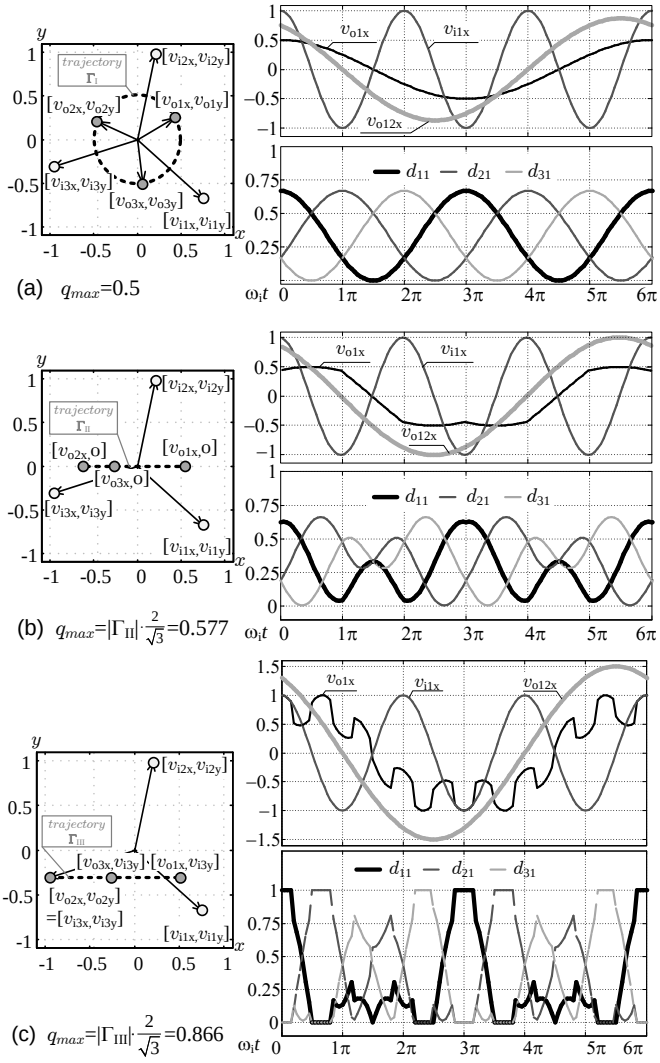


Fig. 5: Example voltage waveforms and the PWM duty cycles for CMC3 $\times$ 3 and $\omega_{\mathrm{i}} = 3\omega_{\mathrm{o}}$ for different types of modulation with: (a) the circular trajectory $\Gamma_{\mathrm{I}}$, (b) centered straight trajectory $\Gamma_{\mathrm{II}}$, (c) shifted straight trajectory $\Gamma_{\mathrm{III}}$ connected with the vertex $v_{\mathrm{i3}}$.

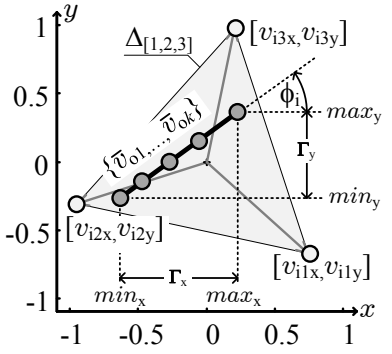


Fig. 6: A straight $\Gamma$ trajectory inclined at an angle of $\phi_{\mathrm{i}}$ inside the synthesis field $\Delta_{[1,2,3]}$.

$\Gamma_{\mathrm{I}}$, shown in Fig. 5(a), the maximum voltage transfer ratio $q_{max}$ is equal to the radius of the circle inscribed in an

equilateral triangle and takes the value $0.5$. By setting each $y$ coordinate value to zero and adding the standard common–mode signal to all $x$ coordinates, the $0.577$ value can be obtained, as illustrated in Fig. 5(b). The last and most important modification consists of the appropriate trajectory $\Gamma_{\rm III}$ shift inside the synthesis field, which allows to reach the $q_{max}$ value equal to $0.866$ – this case is illustrated in Fig. 5(c). For a balanced three–phase source and the input angle $\phi_{\rm i}=0$, the maximum length of the trajectory $\Gamma$, shown is Fig. 6, is equal to the following expression

$$l_{\Gamma\max}=\sqrt{(max_{\rm x}-min_{\rm x})^2+(max_{\rm y}-min_{\rm y})^2}=0.75 \tag{13}$$

Considering the reference non–zero input displacement angle $\phi_{\rm i}$ and $k$ odd number of outputs, the maximum voltage transfer ratio is limited to

$$q_{max}(k,\phi_{\rm i})=\frac{1+\cos\left(\frac{\pi}{3}\right)}{2\cdot\cos\left(\frac{\pi}{2\cdot k}\right)}\cdot\cos\left(\phi_{\rm i}\right) \tag{14}$$

In particular, the applied offset may shift the trajectory $\Gamma$ to the nearest vertex of the voltage synthesis field, which is illustrated in Fig. 5(c). When the two points, which represent the reference and the input voltages overlap each other, the switching is not performed for a certain period of time. In consequence, the total losses can be reduced as a result of this operation. The modulation diagram of the discussed approach is shown in Fig. 8. The proposed concept can be extended to a greater number of converter outputs, which is presented in detail in the next section as the DAV-PWM modulation for CMC with three inputs and odd number of outputs.

## IV. DAV–PWM Modulation for CMC$3\times k$

For three–phase sinusoidal input voltages $v_{\rm i1}$, $v_{\rm i2}$, and $v_{\rm i3}$ the required analytic signals $\overline{\mathbf{v}}_{\rm i}$, can be easy calculated using (5). To increase the maximum voltage transfer ratio $q$ for a given number of outputs and control the input angle $\phi_{\rm i}$, the sinusoidal reference output voltage

$$\mathbf{v}_{\rm o}=q\Big[\ \cos\left(\omega_{\rm o}t\right)\quad\cdots\quad\cos\left(\omega_{\rm o}t-\tfrac{(k-1)2\pi}{k}\right)\ \Big]^T \tag{15}$$

can be converted into the following formula of the modified output analytic voltages

$$\overline{\mathbf{v}}_{\rm o}=(\mathbf{v}_{\rm o}+v_{\rm cm})\cdot\left[\ 1\quad\tan\left(\phi_{\rm i}\right)\ \right] \tag{16}$$

where the common–mode signal $v_{\rm cm}$ is expressed as follows

$$\begin{aligned}&v_{\rm cm}=-0.5(\max_{\rm x}+\min_{\rm x})\\&\max_{\rm x}=\mathrm{MAX}\{v_{\rm o1},v_{\rm o2},...,v_{\rm ok}\}\\&\min_{\rm x}=\mathrm{MIN}\{v_{\rm o1},v_{\rm o2},...,v_{\rm ok}\}\end{aligned} \tag{17}$$

The voltage synthesis field $\Delta_{[1,2,3]}$, input vectors $\overline{\mathbf{v}}_{\rm i}$, and the straight–line $\Gamma$ trajectory with reference analytic voltages $\overline{\mathbf{v}}_{\rm o}$ are shown in Fig. 6. To achieve the maximum voltage transfer ratio (14), the trajectory $\Gamma$ can be shifted to the nearest vertex of the triangle $\Delta_{[1,2,3]}$, as shown in Fig. 5(c), and Fig. 7. This operation can be performed by adding the following coordinates

$$\mathbf{v}_{\rm s}=[v_{\rm sx},v_{\rm sy}] \tag{18}$$

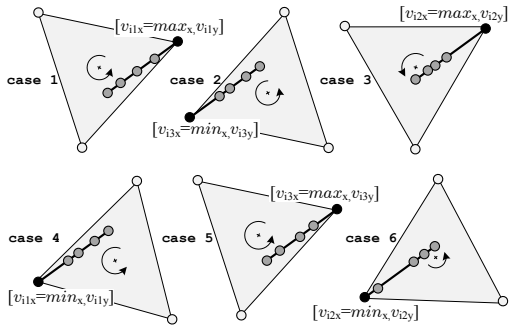


Fig. 7: All possible shift cases of the trajectory $\Gamma$ inside the triangle $\Delta_{[1,2,3]}$.

to each reference voltage pair (16), as illustrated in Fig. 8. Finally, the modulating signals can be written as follows

$$\overline{\mathbf{v}}_{\rm o}=(\mathbf{v}_{\rm o}+v_{\rm cm})\cdot\left[\ 1\quad\tan\left(\phi_{\rm i}\right)\ \right]+\begin{bmatrix}\mathbf{v}_{\rm s}\\ \vdots\\ \mathbf{v}_{\rm s}\end{bmatrix}_{[k\times 2]} \tag{19}$$

where $\mathbf{v}_{\rm s}$ is calculated depending on the $case$, shown in Fig. 7, as follows

$$\begin{aligned}\mathbf{v}_{\rm s1}&=[v_{\rm i1x}-\max_{\rm x},v_{\rm i1y}-\max_{\rm y}]\\ \mathbf{v}_{\rm s2}&=[v_{\rm i3x}-\min_{\rm x},v_{\rm i3y}-\min_{\rm y}]\\ \mathbf{v}_{\rm s3}&=[v_{\rm i2x}-\max_{\rm x},v_{\rm i2y}-\max_{\rm y}]\\ \mathbf{v}_{\rm s4}&=[v_{\rm i1x}-\min_{\rm x},v_{\rm i1y}-\min_{\rm y}]\\ \mathbf{v}_{\rm s5}&=[v_{\rm i3x}-\max_{\rm x},v_{\rm i3y}-\max_{\rm y}]\\ \mathbf{v}_{\rm s6}&=[v_{\rm i2x}-\min_{\rm x},v_{\rm i2y}-\min_{\rm y}]\end{aligned} \tag{20}$$

In the case of balanced voltage source, the proper $case$ can be selected according to the given input voltage sextant shown in Fig. 11. Assuming that all output voltage subscripts start from 4, the required PWM duty cycles matrix $\mathbf{d}_n$ for $n$–output phase can be calculated using the simple formulas (9)–(10), based on barycentric coordinates as follows

$$\mathbf{d}_n=\begin{bmatrix}d_{1n}\\ d_{2n}\\ d_{3n}\end{bmatrix}=\begin{bmatrix}\frac{\Delta_{[n+3,2,3]}}{\Delta_{[1,2,3]}}\\ \frac{\Delta_{[1,n+3,3]}}{\Delta_{[1,2,3]}}\\ \frac{\Delta_{[1,2,n+3]}}{\Delta_{[1,2,3]}}\end{bmatrix} \tag{21}$$

where $n\in\{1,2,3,...,k\}$.

The DAV–PWM modulation diagram for CMC3×3 is shown in Fig. 8, while the algorithm flowchart for CMC3 $\times$ $k$ is presented in Fig. 9. The proposed trajectory shift operation affects the values of the PWM duty cycle matrix elements of the $l$–column, which corresponds to the given converter output

$$\mathbf{D}=\left[\ \mathbf{d}_1\quad\mathbf{d}_2\quad\ldots\quad\mathbf{d}_l\quad\ldots\quad\mathbf{d}_k\ \right] \tag{22}$$

Therefore, the PWM duty cycles for $l$ output can be formally expressed as follows

$$\mathbf{d}_l=\begin{cases}[1,0,0]^T\Leftrightarrow\overline{\mathbf{v}}_{ol}=\overline{\mathbf{v}}_{\rm i1}\\ [0,1,0]^T\Leftrightarrow\overline{\mathbf{v}}_{ol}=\overline{\mathbf{v}}_{\rm i2}\\ [0,0,1]^T\Leftrightarrow\overline{\mathbf{v}}_{ol}=\overline{\mathbf{v}}_{\rm i3}\end{cases} \tag{23}$$

where $l\in\{1,2,3,...,k\}$. It means, that for a certain period of time, one of the input voltage is permanently connected

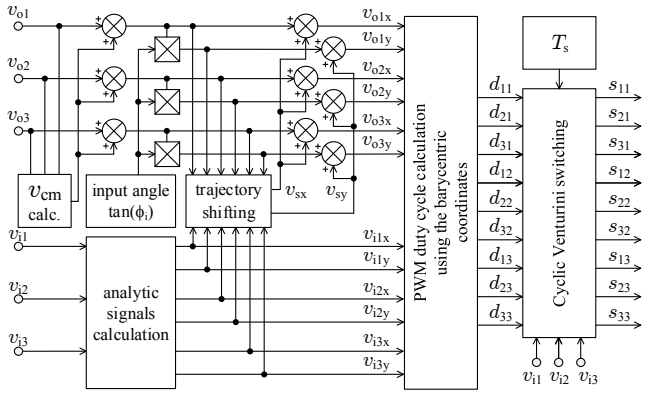


Fig. 8: DAV–PWM modulation diagram for CMC3 $\times$ 3.

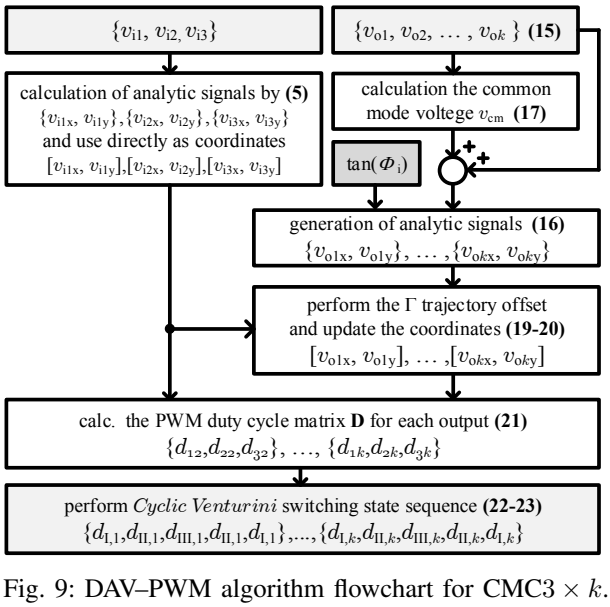


Fig. 9: DAV–PWM algorithm flowchart for CMC3 $\times$ $k$.

with the properly selected converter output, thus the number of switching is also reduced. Example voltages, between the outputs terminal and the neutral point $N$ of the input capacitor star connection, are shown in Fig. 10. Paper [42] compares and presents several PWM signal gating methods. Among them, the Cyclic Venturini and MMM schemes of modulation are proposed. The first method can be implemented by applying the same PWM modulation duty cycles to a double–sided symmetrical switching sequence. This sequence changes cyclically according to the sextant, in which the input voltage space vector lies. The space vector is represented by coordinates $(v_{i\alpha}, v_{i\beta})$ as illustrated in Fig. 11.

When the input voltage source is not purely sinusoidal or balanced, the trajectory shifting operation is performed in a different way. Maintaining the maximum $q$ voltage transfer ratio and the sinusoidal character of the output currents, in the case of an abnormal or distorted voltage source, requires solution for two key problems: proper presentation of all source voltages $\mathbf{v}_i$ – in the meaning of the Hilbert transformation and analytic signal concept – and selection of an optimal $\Gamma$ trajectory position inside the synthesis field $\Delta_{[1,2,3]}$. The first problem has many solutions, among them, the methods

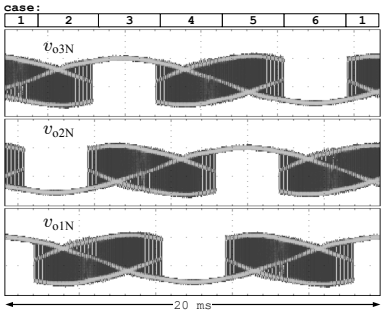


Fig. 10: An example voltage between converter CMC3 $\times$ 3 output and the neutral point $N$ of the input filter capacitor star connection: $q = 0.866$, $\phi_i = 0$, $\omega_o = \omega_i$.

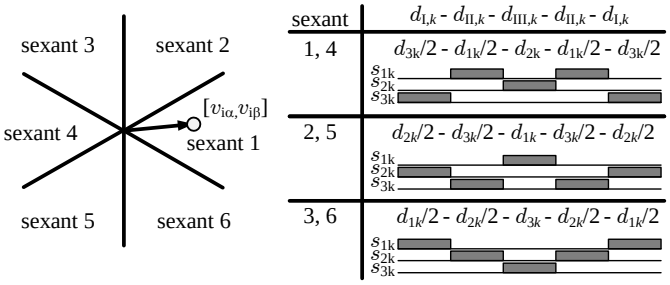


Fig. 11: Cyclic Venturini switching sequence.

based on the Hilbert filter, Fast Fourier Transform or Discrete Fourier Transform can be indicated [34]–[37]. Nowadays, signal processors have hardware support for FFT algorithms in the form of coprocessors and often a special optimized DSP library is available. Nevertheless, taking into account the typical three–phase grid voltage frequency spectrum, the quadrature signals can be calculated selectively by DFT only for the fundamental and $6n\pm1$ harmonics. The general concept of PWM duty cycle computed by (21) remains unchanged. An optimal placement $\Gamma$ trajectory inside the triangle $\Delta_{[1,2,3]}$ can be performed by selecting the smallest control sum $\sigma_r$, calculated for the six cases shown in Fig. 7, as follows

$$\sigma_r = \sigma_{1r} + \sigma_{2r} + \sigma_{3r} \tag{24}$$

where $r \in \{1, 2, 3, 4, 5, 6\}$ and

$$\begin{aligned} \sigma_{1r} &= \left| \det \begin{bmatrix} v_{\mathrm{i2x}} - v_{\mathrm{srx}} & v_{\mathrm{i2y}} - v_{\mathrm{sry}} \\ v_{\mathrm{i3x}} - v_{\mathrm{srx}} & v_{\mathrm{i3y}} - v_{\mathrm{sry}} \end{bmatrix} \right| \\ \sigma_{2r} &= \left| \det \begin{bmatrix} v_{\mathrm{i1x}} - v_{\mathrm{srx}} & v_{\mathrm{i1y}} - v_{\mathrm{sry}} \\ v_{\mathrm{i3x}} - v_{\mathrm{srx}} & v_{\mathrm{i3y}} - v_{\mathrm{sry}} \end{bmatrix} \right| \\ \sigma_{3r} &= \left| \det \begin{bmatrix} v_{\mathrm{i2x}} - v_{\mathrm{srx}} & v_{\mathrm{i2y}} - v_{\mathrm{sry}} \\ v_{\mathrm{i1x}} - v_{\mathrm{srx}} & v_{\mathrm{i1y}} - v_{\mathrm{sry}} \end{bmatrix} \right| \end{aligned} \tag{25}$$

represent determinants calculated for all the shift vector candidates represented by (20). The given $case$ is optimal and finally selected, if the following condition is met

$$case = r \Leftrightarrow \sigma_r = \min\{\sigma_1, \dots, \sigma_6\} \tag{26}$$

The proposed DAV–PWM modulation has two variants of operation:

- the simple variant – input voltage quadrature components are calculated using (5) only and the $\Gamma$ trajectory is shifted according to the sextants illustrated in Fig. 11,
- the advanced variant – analytic signals for the collection of input voltage vectors are computed using the quarter–cycle shifters or advanced technique of signal processing, and the trajectory $\Gamma$ is shifted based on the approach represented by the equations (24) – (26).

In fact, the sinusoidal output current is obtained for both variants of DAV–PWM modulations, and the active power balance is also maintained. The main differences can be observed in the input current shapes during the abnormal input condition, such as amplitude asymmetry as shown in Fig. 12 (waveforms are presented in a per unit format). Input currents are distorted but load currents quality remains unchanged. An effect of advanced variant activation is shown in Fig. 13, where all input currents become sinusoidal waveforms.

The control of the input displacement angle has been analyzed using the mathematical model of the modulation strategy, which is expressed by two following fundamental equations

$$\mathbf{v_o}_{[1\times k]} = \mathbf{v_i}_{[1\times 3]} \cdot \mathbf{D}_{[3\times k]} \tag{27}$$

$$\mathbf{i_i}_{[1\times 3]} = \mathbf{i_o}_{[1\times k]} \cdot \mathbf{D}^T_{[k\times 3]} \tag{28}$$

Assuming the three–phase sinusoidal output currents with amplitude $I_\mathrm{o}$, and a load angle $\varphi_\mathrm{o}$

$$\mathbf{i}_\mathrm{o} = \begin{bmatrix} i_{\mathrm{o}1} \\ i_{\mathrm{o}2} \\ i_{\mathrm{o}3} \end{bmatrix} = I_\mathrm{o} \cdot \begin{bmatrix} \cos\left(\omega_\mathrm{o} t + \varphi_\mathrm{o}\right) \\ \cos\left(\omega_\mathrm{o} t + \varphi_\mathrm{o} - 2\pi/3\right) \\ \cos\left(\omega_\mathrm{o} t + \varphi_\mathrm{o} + 2\pi/3\right) \end{bmatrix} \tag{29}$$

the more practical expression of the input currents can be elaborated using (28) and the Clarke transform, which results in the following formula

$$\begin{aligned} i_{\mathrm{i}\alpha} &= I_\mathrm{i} \cdot \left(\cos\left(\omega_\mathrm{i} t\right) - \tan\left(\phi_\mathrm{i}\right) \cdot \sin\left(\omega_\mathrm{i} t\right)\right) \\ i_{\mathrm{i}\beta} &= I_\mathrm{i} \cdot \left(\sin\left(\omega_\mathrm{i} t\right) + \tan\left(\phi_\mathrm{i}\right) \cdot \cos\left(\omega_\mathrm{i} t\right)\right) \end{aligned} \tag{30}$$

where

$$I_\mathrm{i} = q \cdot I_\mathrm{o} \cdot \cos\left(\varphi_\mathrm{o}\right) \tag{31}$$

The above equations for CMC3$\times$3 have been elaborated using the Math Symbolic Toolbox, where all elements of matrix D have been presented as a ratio of triangles according to the (9) – (11), and (21). The approach allows to realize an algorithm for any outputs number $k$ and desired input angle $\phi_\mathrm{i}$. Simulation results of DAV–PWM modulation for CMC3$\times$5 and CMC3$\times$11 are shown in Fig. 14 and Fig. 15 respectively. Most important simulation parameters are listed in Table I.

TABLE I: Simulation parameters used in PSIM11 software.

| Parameter | Value |
|---|---|
| Source phase-to-phase voltage | $V_\mathrm{i} = 100\mathrm{V}$ |
| Input frequency | $f_\mathrm{i} = 50\mathrm{Hz}$ |
| Input filter | $C_f = 15\mu\mathrm{F}$, $L_f = 200\mu\mathrm{H}$ |
| Cabling resistance | $R_f = 0.1\Omega$ |
| PWM sampling frequency | $f_s = 10\mathrm{kHz}$ |
| RL load parameters | $R = 0.5\Omega$, $L = 8.3\mathrm{mH}$ |

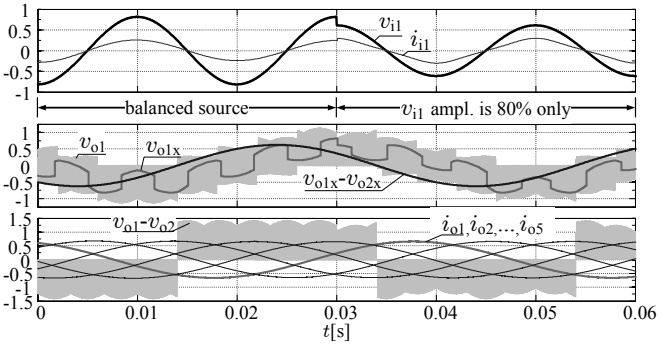


Fig. 12: An illustration of rapid change of an input voltage amplitude: CMC3 $\times$ 5 converter, $\phi_\mathrm{i} = 0$, $q = 0.65$.

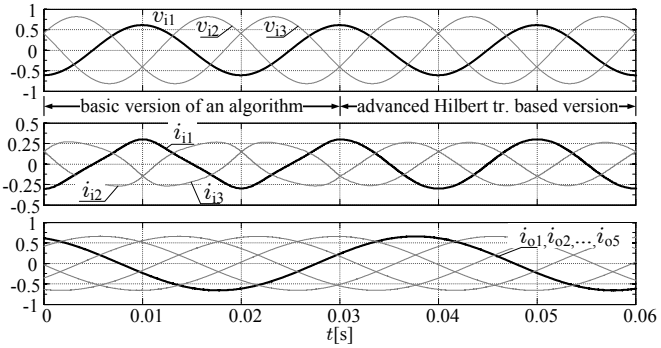


Fig. 13: An effect of advanced variant of DAV–PWM activation.

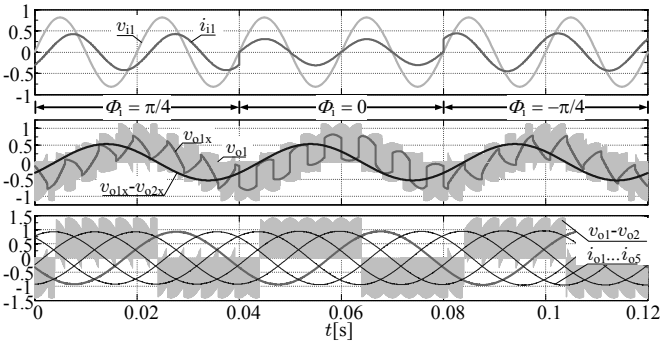


Fig. 14: An input angle control of CMC3 $\times$ 5 converter for $\phi_\mathrm{i} = \{\pi/4, 0, -\pi/4\}$: $q = \cos\left(\pi/4\right)\left(0.75/\cos\left(\pi/10\right)\right)$.

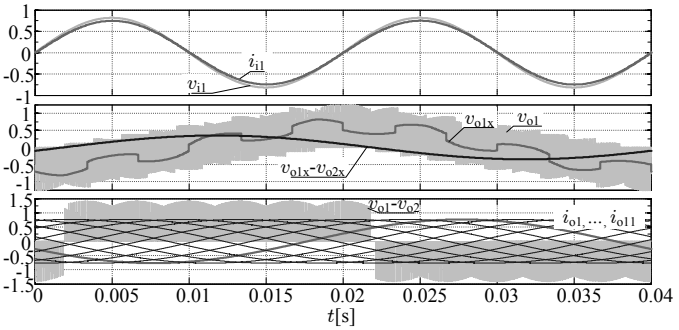


Fig. 15: The control of CMC3 $\times$ 11 converter under unity power factor operation: $\phi_\mathrm{i} = 0$, $q = q_{max} = 0.757$.

## V. Smooth Interpolation Method

Multiphase sources can be represented as a set of rotating vectors by conversion of the sampled voltages into the analytic signals. Each voltage is expressed as a pair of two elements – $real$ and $imaginary$, which correspond to the $x$ and $y$ coordinates of vertices the convex polygon. This polygon, with the number of vertices $N \geq 3$, rotates and is the voltage synthesis field. All output vectors, inside the synthesis field, can be also represented by analytic signals. The movement of each reference output voltage inside a synthesis field can be graphically represented by $trajectory$, which can be a circle or straight line in particular. The position of each point inside the synthesis field can be expressed by the Wachspress coordinates, which are relatively simple rational functions. The value of the mathematical relation – in the meaning of PWM duty cycles value – between any internal point and all vertices of the synthesis field can be determined using the smooth interpolation. This approach can be successfully adopted for PWM modulation [40], and can be applied for AC–AC voltage conversion as well.

Let's assume, that a point $p_\mathrm{o}$ represents the analytic output voltage and lies inside the synthesis field shown in Fig. 16(a). PWM duty cycle for $\bar{v}_{\mathrm{i}m}$ input phase, which corresponds to the $p_m$ vertex, can be computed using Wachspress formula

$$d\left(p_m\right) = \frac{w_m\left(p_\mathrm{o}, p_m\right)}{\sum\limits_{k=1}^{N} w_k\left(p_\mathrm{o}, p_k\right)} \tag{32}$$

where the numerator is the weight calculated as follows

$$w_m\left(p_\mathrm{o}, p_m\right) = \frac{\Delta\left[p_{m-1}, p_m, p_{m+1}\right]}{\Delta\left[p_{m-1}, p_m, p_\mathrm{o}\right] \cdot \Delta\left[p_\mathrm{o}, p_m, p_{m+1}\right]} \tag{33}$$

According to the Wachspress approach properties [43], [44], the sum of all calculated duty cycles is equal unity

$$\sum_{k=1}^{N} d\left(p_k\right) = 1 \tag{34}$$

and in particular,

$$d\left(p_m\right) = 1 \Leftrightarrow p_m = p_\mathrm{o} \tag{35}$$

It should be pointed out that the voltage synthesis field does not have to contain all input voltages, but only selected ones. Thus, the size of the subset of input voltages can be dynamically changed i.e. during an unexpected fault. An example voltage vector diagram of the six–phase system, which is connected with CMC6 × 6 is shown in Fig. 16(b). An example output vector $\vec{v}_{\mathrm{o}1}$ represents the purely sinusoidal reference voltage, thus the shown trajectory $\Gamma_\mathrm{o}$ is a circle. A PWM duty cycle waveform $d_1$, calculated for $v_{\mathrm{i}1}$, is shown in Fig. 17, where the input voltage is intentionally distorted by known higher–order harmonics to demonstrate that the output voltage is correctly synthesized and the output currents $i_{\mathrm{o}1\ldots\mathrm{o}6}$ remain sinusoidal – this is an advantage of the proposed approach. If the number of input vectors is 3, formula (32) is reduced to the relation of two triangle areas as expressed by (21). The smooth interpolation method can be used for CMC converters where the number of inputs is greater, equal to the number of outputs.

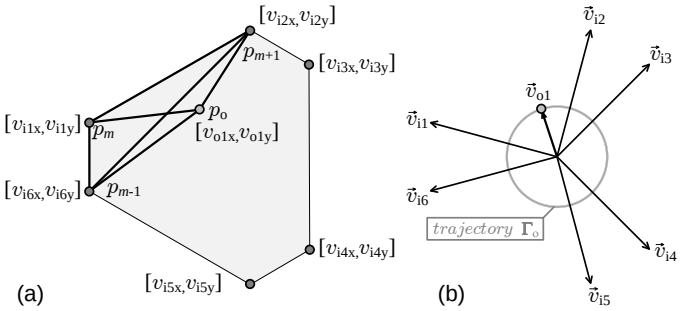


Fig. 16: Application of the Wachspress coordinates for CMC6 × 6: (a) synthesis field, (b) six input voltage vectors.

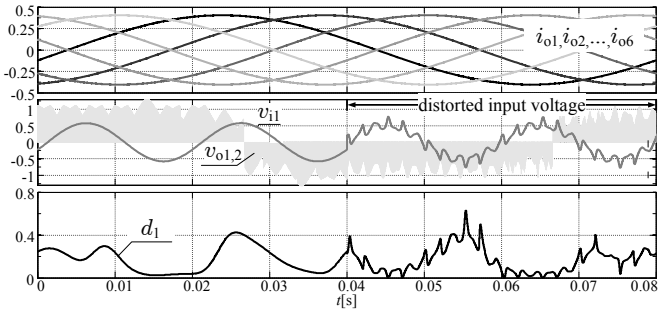


Fig. 17: CMC6 × 6: $q = 0.6$ and $\omega_\mathrm{i} = 4\omega_\mathrm{o}$, $RL$ type load, $v_{\mathrm{o}1,2}$ load line–to–line voltage, $i_{\mathrm{o}1\ldots\mathrm{o}6}$ load currents, $v_{\mathrm{i}1}$ input voltage, $d_{11}$ PWM duty cycle.

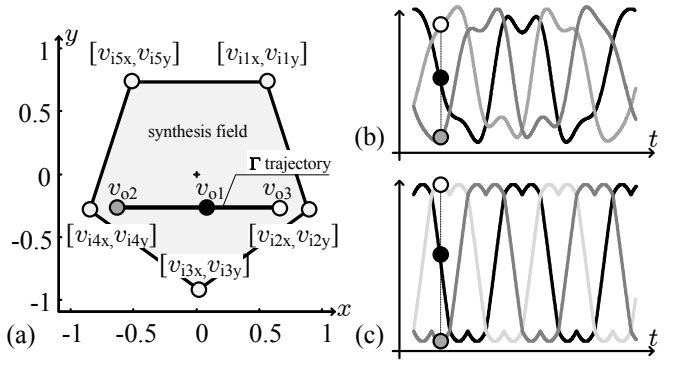


Fig. 18: An illustration of the example modulation scenario, which uses the straight–line shape of the trajectory Γ for CMC5 × 3: (a) synthesis field, (b) reference output voltages based on Venturini generalized approach from [23], (c) sinusoidal reference with common–mode signal injection.

If a maximum value of $q$ is needed, a straight–line trajectory Γ can be applied, as shown in Fig. 18(a). The reference output voltage can be selected arbitrarily for maximizing the peak–to–peak line–to–line voltage. The Optimum–Venturini and the sinusoidal, with common–mode signal injection, references are illustrated in Fig. 18(b) and Fig. 18(c) respectively. The algorithm flowchart is the same as in Fig. 9, only number of the input voltages is changed. More research on multiphase CMC will be discussed in detail in a separate paper.

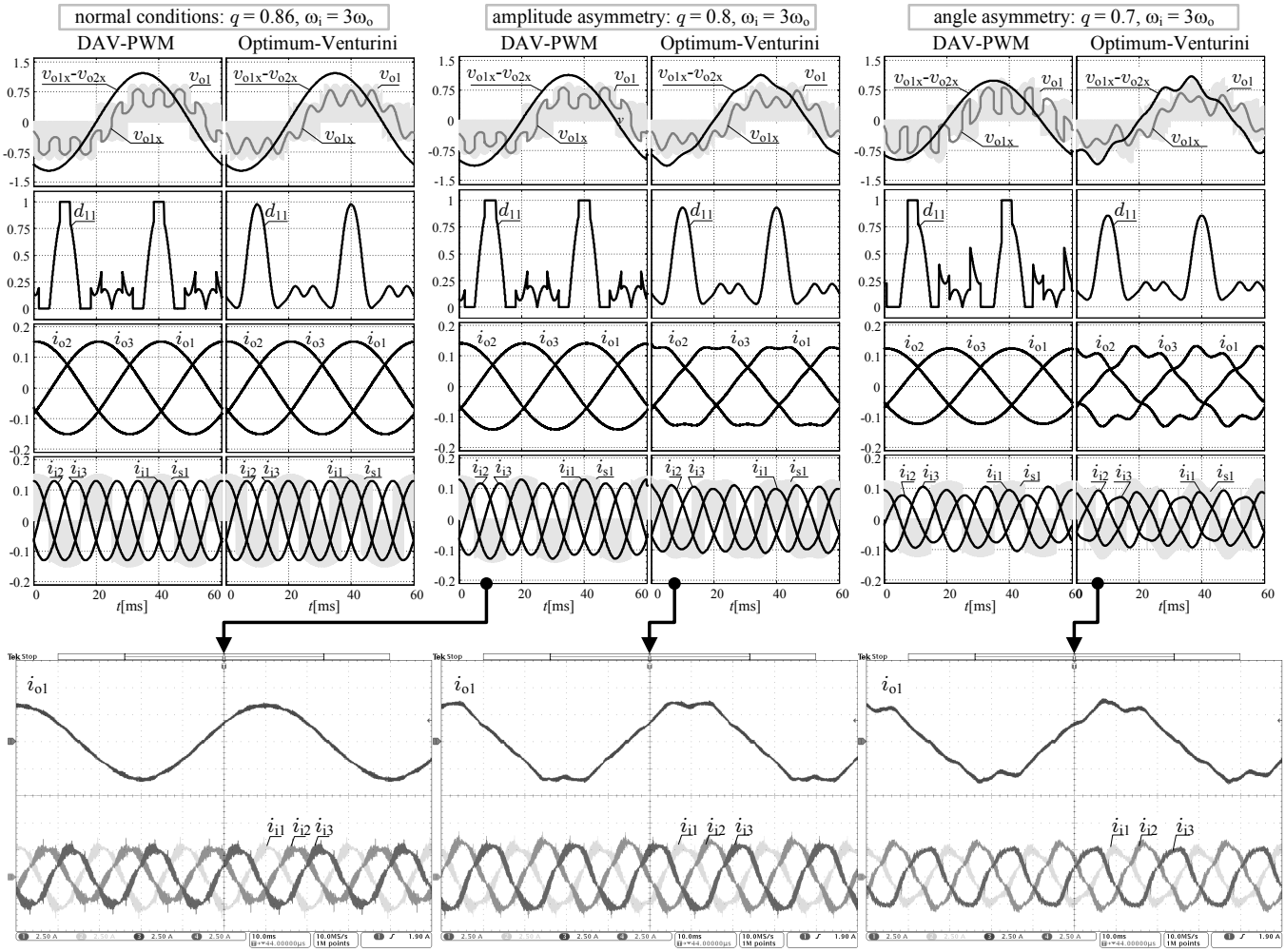


Fig. 19: The comparison of the proposed advanced variant of DAV–PWM and the Optimum–Venturini for three example input voltage conditions and $\phi_i = 0$.

## VI. Simulation results

Some simulation results have been partially presented in section IV. Non–sinusoidal input waveforms, such as rectangular or distorted by the higher–order voltage harmonics have been analyzed through simulation. The DAV–PWM modulation has been also compared with the Optimum Venturini direct modulation method.

### *Comparison with the Optimum–Venturini direct modulation method for CMC* $3 \times 3$

The proposed modulation approach is a direct method of modulation and can be compared with the Optimum–Venturini solution. This method is used to generate variable frequency and amplitude sinusoidal output voltage $v_{jN}$ from the fixed–frequency, fixed–amplitude input voltage $v_{iN}$ with the amplitude $\mathrm{V_i}$, where $j = a, b, c$ indicates CMC outputs, while $i = A, B, C$ denotes the CMC input. The $d_{ij}(t)$ PWM duty cycle can be calculated using the following expression

$$d_{ij} = \frac{1}{3}\left(1 + \frac{2v_{iN}(t)\,\bar{v}_{jN}}{\mathrm{V_i^2}} + \frac{4q}{3\sqrt{3}}\zeta\right) \tag{36}$$

where the modulating signal $\bar{v}_{jN}$ represents the mean value of the output voltage, $\zeta = \sin(\omega_i t + \beta_i)\sin(3\omega_i t)$, and $\beta_i = 0, (2\pi/3), (4\pi/3)$. To increase the gain voltage to $q = 0.866$ Venturini proposed the injection of a third harmonic, thus in the Optimum–Venturini approach, modulating signals are expressed as follows

$$v_{jN}(t) = q\mathrm{V_i}\left(\cos(\omega_o t + \alpha_o) - \zeta_o\right) \tag{37}$$

where $\zeta_o = \frac{\cos(3\omega_o t)}{6} - \frac{\cos(3\omega_i t)}{2\sqrt{3}}$ and $\alpha_o = 0, (2\pi/3), (4\pi/3)$.

The comparison for simulation and experiment, shown in Fig. 19, has been performed for normal supply conditions, $20\%$ amplitude asymmetry, and the $\pi/6$ angle asymmetry of one source voltage. The presented simulation results and oscillogram collection confirm the positive features of the proposed method of modulation such as maintaining the sinusoidal input and output currents during the abnormal supply condition. Due to observed currents distortion in the case of the Optimum–Venturini method, the conclusion is that the method is not suitable for such conditions and the robustness of the DAV–PWM modulation is proved. Comparative tests were carried out using the regulated AC voltage source ($30V$–$50V$)

specially equipped with a and RL load ($R = 8\Omega$, $L = 6mH$). Practical conditions have been faithfully reproduced in the simulation using the PSIM11, with the algorithm frequency equal to the $10kHz$.

### *Non-sinusoidal input waveforms case*

Using the proposed advanced variant of modulation, the sinusoidal output current has been generated properly even if the input voltages contained higher–order harmonics, shown in Fig. 20. Changing the amplitude of one of the input voltages causes the supply asymmetry, which translates into the deformation of the synthesis field, so the triangle, shown in Fig. 6, is not equilateral in this case. If the reference voltages still lie inside the synthesis field, all output voltages will also be generated properly, which illustrated in Fig. 12. Theoretically, by using equation (5), the proposed approach can be used for any symmetric, balanced three–phase source such as rectangular voltages. This case has been illustrated in Fig. 21 and Fig. 22. In this particular supply case, a pure sinusoidal output current has been also obtained. The triangle $\Delta_{[1,2,3]}$ rotates discretely, i.e. its position in the $xy$ coordinate system is fixed within one of the six rotation cycles. Such type of voltage supply also allows for achieving a higher $q_{max} = 2/\sqrt{3}$. This result is presented only as a demonstration of the capability of the proposed approach.

## VII. Experimental results

The developed DAV–PWM modulation has been tested for CMC3 $\times$ 3 and CMC3 $\times$ 5. In the first case, the experiments have been performed for a three–phase $RL$ loads. The prototype of the CMC3 $\times$ 3 converter and control board are shown in Fig. 23. The solution for the CMC3 $\times$ 5 has been verified using a 5kW/140V five–phase squirrel–cage motor, shown in Fig. 24, and two converters $\mathrm{CMC}_1$ and $\mathrm{CMC}_2$. The proposed algorithm has been implemented with floating–point multicore digital signal processor Analog Devices ADSP–SC589. A programmable logic devices Intel FPGA MAX10 has been used mainly for perform the four–step commutation and analog–to–digital signal conversion. System commands and other operations have been served using additional software, which operated via fiber optic.

Typical waveforms for the simple variant of the DAV–PWM modulation for CMC3$\times$3 fed by balanced three–phase voltage source are shown in Fig. 25. Presented results confirm the correct regulation of the load voltage and the input angle. The proposed advanced variant of DAV–PWM has been tested during the amplitude asymmetry of the voltage source, which is presented in one of the oscillograms shown in Fig. 19, where both the input and the output currents remained undistorted. The proposed modulation algorithms for a converter with five outputs – the simple modulation variant and the advanced one – have been also verified in the same abnormal source condition. The effects are presented in Fig. 26, where the input current for both DAV–PWM variants and obtained sinusoidal load currents have been shown.

Assuming potential use of the proposed method in multi-phase high–frequency applications, the high-performance DSP

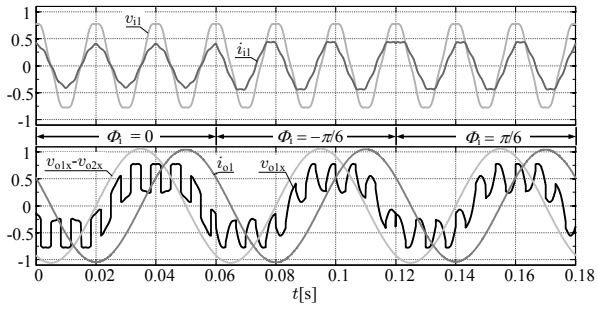


Fig. 20: The changes of input current angle for CMC3 $\times$ 3 during harmonic distortion of the input voltage: $\omega_\mathrm{i} = 3\omega_\mathrm{o}$, $\phi_\mathrm{i} = \{0, -\pi/6, \pi/6\}$.

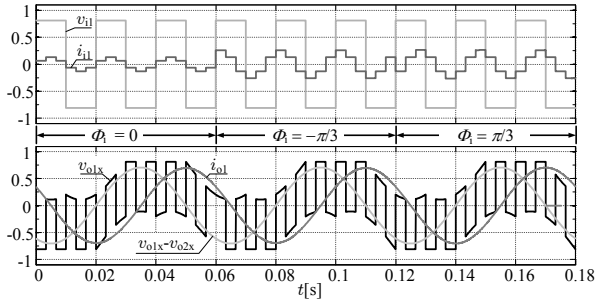


Fig. 21: Control of CMC3 $\times$ 3 converter fed by three–phase rectangular source: $q = 0.5$, $\phi_\mathrm{i} = \{0, -\pi/3, \pi/3\}$, $\omega_\mathrm{i} = 3\omega_\mathrm{o}$.

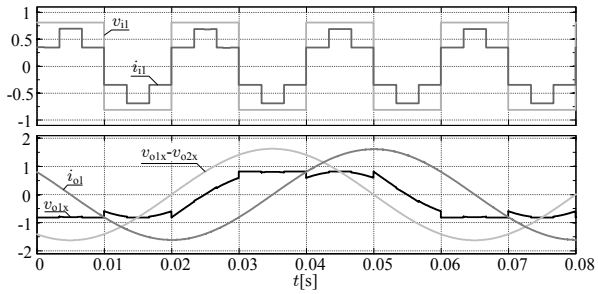


Fig. 22: Control of CMC3 $\times$ 3 converter with three–phase rectangular voltage supply: $q = 1.1$, $\phi_\mathrm{i} = 0$, $\omega_\mathrm{i} = 3\omega_\mathrm{o}$.

processor TMS320C6672-1GHz has been selected for the benchmark, which number of CPU cycles has been measured by a special timestamp timer. All algorithms in the benchmark have been designed and programmed using special math functions from the DSP library, thus the standard C functions have not been applied. Results are presented in Tab. II.

TABLE II: Comparison of the number of TMS320C6672 1GHz processor CPU cycles for selected algorithms.

| Algorithm | Cycles |
|---|---|
| Classic Venturini, $q_{max} = 0.5$ | 337 |
| Extended Venturini, $q_{max} = 0.866$ | 2038 |
| DAV–PWM with the circle trajectory, $q_{max} = 0.5$ | 224 |
| DAV–PWM with the straight–line trajectory, $q_{max} = 0.866$ | 259 |
| DAV–PWM with the straight–line shifted trajectory | 548 |

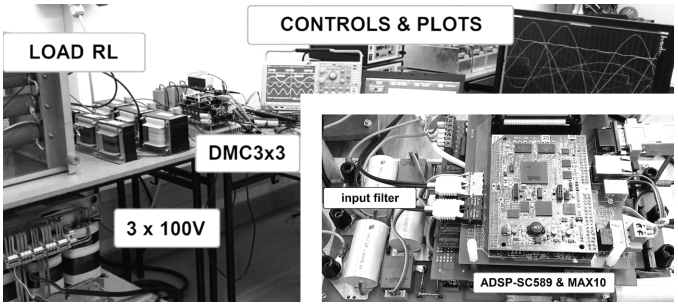


Fig. 23: CMC3 $\times$ 3 and control board.

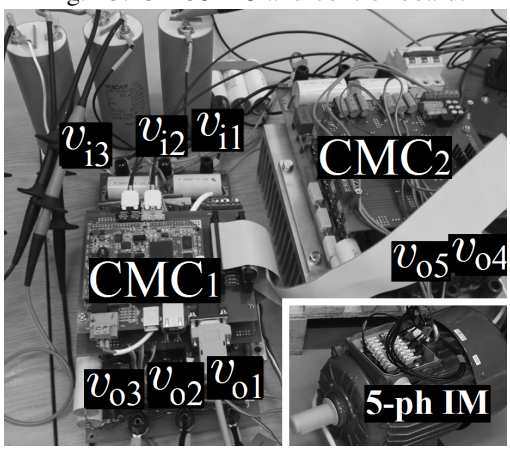


Fig. 24: The model of CMC3 $\times$ 5 converter connected with the 5–phase, 5kW squirrel cage engine prototype.

## VIII. Conclusion

The use of analytical signal and smooth interpolation in AC–AC voltage synthesis facilitates modulation algorithm prototyping. Although the vector terminology still appears in the proposed method description, the idea of computing the PWM duty cycle is free from trigonometry and angles, which in consequence accelerates the calculation. The discussed approach can be used under the wide range of input voltage conditions, starting from amplitude asymmetry, ending with the radical voltage waveform shape change. Voltages presentation using an analytic signal, is intuitive and can express almost all input voltage conditions. However, as discussed in the paper, it can require advanced harmonic analysis but nowadays it is strongly supported, both in hardware and software. The PWM duty cycle can be computed based on the barycentric coordinates using the ratio of triangle areas or applying the smooth interpolation by Wachspress formula. The PWM duty cycle can be computed using the barycentric coordinates using the ratio of triangle areas or applying the smooth interpolation using the Wachspress formula. The presented solution, in particular, the barycentric coordinates, can be adopted to develop a solution for other multiphase matrix converters, such as multipulse matrix converters, which is the aim of further research.

## References

[1] L. Empringham, J. Kolar, J. Rodriguez, P. Wheeler, and J. C. Clare, "Technological issues and industrial application of matrix converters: A review," *IEEE Trans. Ind. Electron.*, vol. 60, DOI 10.1109/TIE.2012.2216231, no. 10, pp. 4260–4271, Oct. 2013.

[2] C. Klumpner, P. Nielsen, I. Boldea, and F. Blaabjerg, "A new matrix converter motor (mcm) for industry applications," *IEEE Trans. Ind. Electron.*, vol. 49, no. 2, pp. 325–335, Apr. 2002.

[3] M. Venturini and A. Alesina, "The generalised transformer: A new bidirectional, sinusoidal waveform frequency converter with continuously adjustable input power factor," in *1980 IEEE Power Electronics Specialists Conference*, DOI 10.1109/PESC.1980.7089455, pp. 242–252, Jun. 1980.

[4] A. Alesina and M. G. B. Venturini, "Analysis and design of optimum-amplitude nine-switch direct ac-ac converters," *IEEE Transactions on Power Electronics*, vol. 4, DOI 10.1109/63.21879, no. 1, pp. 101–112, Jan. 1989.

[5] T. Friedli and J. Kolar, "Milestones in matrix converter research," *IEEJ Journal of Industry Application*, vol. 1, DOI 10.1541/ieejjia.1.2, no. 1, pp. 2–14, Jul. 2012.

[6] A. K. Dey, G. Mohapatra, T. K. Mohapatra, and R. Sharma, "A modified venturini pwm scheme for matrix converters," in *2019 IEEE International Conference on Sustainable Energy Technologies and Systems (ICSETS)*, DOI 10.1109/ICSETS.2019.8745014, pp. 013–018, Feb. 2019.

[7] J. Rodriguez, M. Rivera, J. Kolar, and P. Wheeler, "A review of control and modulation methods for matrix converters," *IEEE Trans. Ind. Electron.*, vol. 59, DOI 10.1109/TIE.2011.2165310, no. 1, pp. 58–70, Jan. 2012.

[8] Z. Malekjamshidi, M. Jafari, and J. Zhu, "Analysis and comparison of direct matrix converters controlled by space vector and venturini modulations," in *2015 IEEE 11th International Conference on Power Electronics and Drive Systems*, DOI 10.1109/PEDS.2015.7203550, pp. 635–639, Jun. 2015.

[9] S. M. Ahmed, Z. Salam, and H. Abu-Rub, "An improved space vector modulation for a three-to-seven-phase matrix converter with reduced number of switching vectors," *IEEE Trans. Ind. Electron.*, vol. 62, DOI 10.1109/TIE.2014.2381158, no. 6, pp. 3327–3337, Dec. 2015.

[10] S. M. Ahmed, A. Iqbal, H. Abu-Rub, J. Rodriguez, C. Rojas, and M. Saleh, "Simple carrier-based pwm technique for a three-to-nine phase direct ac-ac converter," *IEEE Trans. Ind. Electron.*, vol. 58, DOI 10.1109/TIE.2011.2134062, no. 11, pp. 5014–5023, Nov. 2011.

[11] S. M. Ahmed, A. Iqbal, and H. Abu-Rub, "Generalized duty-ratio-based pulsewidth modulation technique for a three-to-k phase matrix converter," *IEEE Trans. Ind. Electron.*, vol. 58, DOI 10.1109/TIE.2010.2098373, no. 9, pp. 3925–3937, Sep. 2011.

[12] T. D. Nguyen and H. Lee, "Development of a three-to-five-phase indirect matrix converter with carrier-based pwm based on space-vector modulation analysis," *IEEE Trans. Ind. Electron.*, vol. 63, DOI 10.1109/TIE.2015.2472359, no. 1, pp. 13–24, Sep. 2016.

[13] P. Zanchetta, P. Wheeler, J. Clare, M. Bland, L. Empringham, and D. Katsis, "Control design of a three-phase matrix-converter-based ac-ac mobile utility power supply," *IEEE Trans. Ind. Electron.*, vol. 55, DOI 10.1109/TIE.2007.903974, no. 1, pp. 209–217, Jan. 2008.

[14] X. Liu, P. Wang, P. Loh, and F. Blaabjerg, "A three-phase dual-input matrix converter for grid integration of two ac type energy resources," *IEEE Trans. Ind. Electron.*, vol. 60, DOI 10.1109/TIE.2012.2183838, no. 1, pp. 20–29, Jan. 2013.

[15] M. Y. Lee, P. Wheeler, and C. Klumpner, "Space-vector modulated multilevel matrix converter," *IEEE Trans. Ind. Electron.*, vol. 57, DOI 10.1109/TIE.2009.2038940, no. 10, pp. 3385–3394, Oct. 2010.

[16] R. Pena, R. Cardenas, E. Reyes, J. Clare, and P. Wheeler, "Control of a doubly fed induction generator via an indirect matrix converter with changing dc voltage," *IEEE Trans. Ind. Electron.*, vol. 58, DOI 10.1109/TIE.2011.2109334, no. 10, pp. 20–29, Oct. 2011.

[17] L. Helle, K. Larsen, A. Jorgensen, S. Munk-Nielsen, and F. Blaabjerg, "Evaluation of modulation schemes for three-phase to three-phase matrix converters," *IEEE Trans. Ind. Electron.*, vol. 51, DOI 10.1109/TIE.2003.821900, no. 1, pp. 158–171, Feb. 2004.

[18] U. Nasir, A. Costabeber, P. Wheeler, and M. Rivera, "A new ac/ac power converter," in *2017 IEEE Southern Power Electronics Conference (SPEC)*, DOI 10.1109/SPEC.2017.8333649, pp. 1–6, Dec. 2017.

[19] P. Boonseam, N. Jarutus, and Y. Kumsuwan, "A control strategy for a matrix converter based on venturini method under unbalanced input voltage conditions," in *2016 13th International Conference on Electrical Engineering/Electronics, Computer, Telecommunications and Information Technology (ECTI-CON)*, DOI 10.1109/ECTICon.2016.7561471, pp. 1–6, Jun. 2016.

[20] W. Xiong, Y. Sun, J. Lin, M. Su, H. Dan, M. Rivera, and J. M. Guerrero, "A cost-effective and low-complexity predictive control for matrix

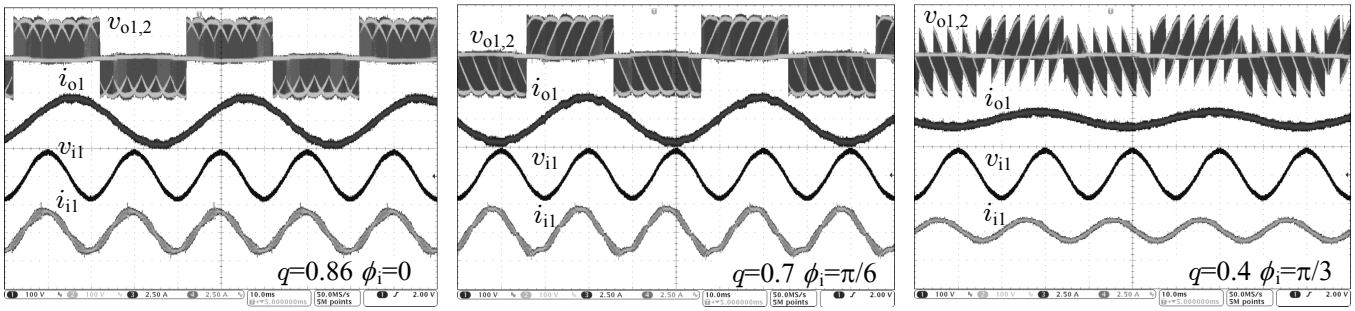


Fig. 25: Typical waveforms for DAV–PWM modulation applied to the CMC3 × 3: $\omega_o = 0.5\omega_i$, load $R = 30\Omega$, $L = 9m$.

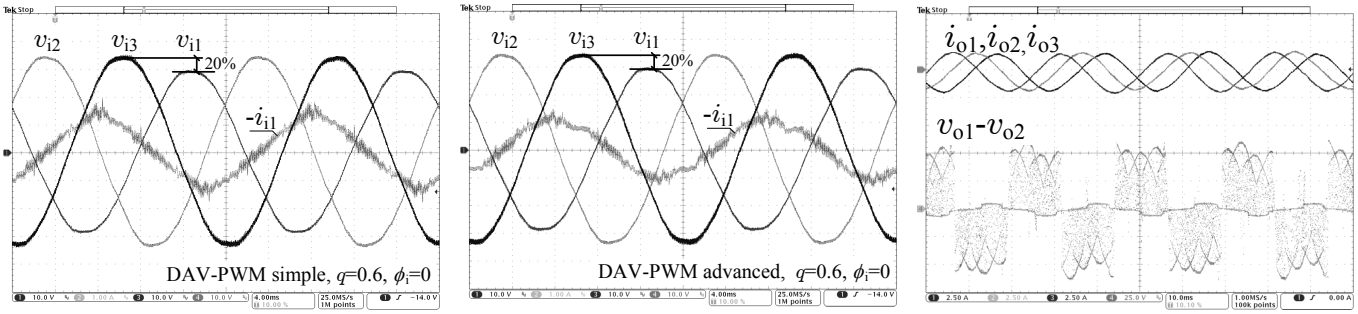


Fig. 26: A 5–phase IM supplied by CMC3 × 5 during the 20% of input voltage asymmetry: $q = 0.6$, $\phi_i = 0$, $\omega_o = 0.8\omega_i$.

converters under unbalanced grid voltage conditions," *IEEE Access*, vol. 7, DOI 10.1109/ACCESS.2019.2908446, pp. 43 895–43 905, 2019.

[21] X. Wang, H. Lin, H. She, and B. Feng, "A research on space vector modulation strategy for matrix converter under abnormal input-voltage conditions," *IEEE Trans. Ind. Electron.*, vol. 59, DOI 10.1109/TIE.2011.2157288, no. 1, pp. 93–104, Jan. 2012.

[22] O. Abdel-Rahim, H. Funato, H. Abu-Rub, and O. Ellabban, "Multi-phase wind energy generation with direct matrix converter," in *2014 IEEE International Conference on Industrial Technology (ICIT)*, DOI 10.1109/ICIT.2014.6894994, pp. 519–523, Feb. 2014.

[23] M. Ali, A. Iqbal, M. R. Khan, M. Ayyub, and M. A. Anees, "Generalized theory and analysis of scalar modulation techniques for a $m \times n$ matrix converter," *IEEE Transactions on Power Electronics*, vol. 32, DOI 10.1109/TPEL.2016.2600034, no. 6, pp. 4864–4877, Jun. 2017.

[24] M. Ali, A. Iqbal, M. Anas Anees, M. Rizwan Khan, K. Rahman, and M. Ayyub, "Differential evolution-based pulse-width modulation technique for multiphase mc," *IET Power Electronics*, vol. 12, DOI 10.1049/iet-pel.2018.5862, no. 9, pp. 2224–2235, 2019.

[25] S. Pipolo, A. Formentini, A. Trentin, P. Zanchetta, M. Calvini, and M. Venturini, "A new modulation approach for matrix converter," in *2019 10th International Conference on Power Electronics and ECCE Asia (ICPE 2019 - ECCE Asia)*, pp. 1021–1027, May. 2019.

[26] M. Ishida, T. Ueda, T. Tanaka, and D. Ueda, "Gan on si technologies for power switching devices," *IEEE Transactions on Electron Devices*, vol. 60, DOI 10.1109/TED.2013.2268577, no. 10, pp. 3053–3059, Oct. 2013.

[27] D. Lan, P. Das, and S. K. Sahoo, "A high-frequency link matrix rectifier with a pure capacitive output filter in a discontinuous conduction mode," *IEEE Transactions on Industrial Electronics*, vol. 67, DOI 10.1109/TIE.2019.2893838, no. 1, pp. 4–15, Jan. 2020.

[28] R. J. Kaplar, M. J. Marinella, S. DasGupta, M. A. Smith, S. Atcitty, M. Sun, and T. Palacios, "Characterization and reliability of sic- and gan-based power transistors for renewable energy applications," in *2012 IEEE Energytech*, DOI 10.1109/EnergyTech.2012.6304627, pp. 1–6, May. 2012.

[29] L. Keuck, P. Hosemann, B. Strothmann, and J. Boecker, "A comparative study on si-sj-mosfets vs. gan-hemts used for llc-single-stage battery charger," in *PCIM Europe 2017; International Exhibition and Conference for Power Electronics, Intelligent Motion, Renewable Energy and Energy Management*, pp. 1–8, May. 2017.

[30] K. Kumar, M. Bhattacharya, S. Garlapati, and S. Banerjee, "Impact of gallium nitride semiconductor devices in tri-state boost converter," in *2019 IEEE International Conference on Sustainable Energy Technologies and Systems (ICSETS)*, DOI 10.1109/ICSETS.2019.8744791, pp. 292–296, Feb. 2019.

[31] A. Taylor, J. Lu, L. Zhu, K. Bai, M. McAmmond, and A. Brown, "Comparison of sic mosfet-based and gan hemt-based high-efficiency high-power-density 7.2 kw ev battery chargers," *IET Power Electronics*, vol. 11, DOI 10.1049/iet-pel.2017.0467, no. 11, pp. 1849–1857, 2018.

[32] N. He, M. Chen, J. Wu, N. Zhu, and D. Xu, "20-kw zero-voltage-switching sic-mosfet grid inverter with 300 khz switching frequency," *IEEE Transactions on Power Electronics*, vol. 34, DOI 10.1109/T-PEL.2018.2866824, no. 6, pp. 5175–5190, Jun. 2019.

[33] T. Hirota, K. Inomata, D. Yoshimi, and M. Higuchi, "Nine switches matrix converter using bi-directional gan device," in *2018 International Power Electronics Conference (IPEC-Niigata 2018 -ECCE Asia)*, DOI 10.23919/IPEC.2018.8507399, pp. 3952–3957, May. 2018.

[34] G. Todoran and R. Holonec, "Analysis of the multi-phased system based on the concept of analytic signals," *4th International Conference on Power Engineering, Energy and Electrical Drives*, DOI 10.1109/PowerEng.2013.6635689, May. 2013.

[35] C. Rader, "A simple method for sampling in-phase and quadrature components," *IEEE Aerosp. Electron. Syst. Mag.*, vol. AES-20, DOI 10.1109/TAES.1984.310466, no. 6, pp. 821–824, Nov. 1984.

[36] A. Reilly, G. Frazer, and B. Boashash, "Analytic signal generation-tips and traps," *IEEE Trans. Signal Process.*, vol. 42, DOI 10.1109/78.330385, no. 11, pp. 3241–3245, Nov. 1994.

[37] L. Marple, "Computing the discrete-time "analytic" signal via fft," *IEEE Trans. Signal Process.*, vol. 47, DOI 10.1109/78.782222, no. 9, pp. 2600–2603, Sep. 1999.

[38] L. Asiminoael, F. Blaabjerg, and S. Hansen, "Computing the discrete-time "analytic" signal via fft," *IEEE Ind. Appl. Mag.*, vol. 13, DOI 10.1109/MIA.2007.4283506, no. 4, pp. 22–33, Jul. 2007.

[39] H. Hojabri, H. Mokhtari, and L. Chang, "A generalized technique of modeling, analysis, and control of a matrix converter using svd," *IEEE Trans. Ind. Electron.*, vol. 58, DOI 10.1109/TIE.2010.2048836, no. 3, pp. 949–959, Mar. 2011.

[40] P. Szczepankowski and J. Nieznanski, "Application of barycentric coordinates in space vector pwm computations," *IEEE Access*, DOI 10.1109/ACCESS.2019.2914854, 2019.

[41] D. Casadei, G. Serra, A. Tani, and L. Zarrir, "Matrix converter modulation strategies: A new general approach based on space-vector representation of the switch state," *IEEE Trans. Ind. Electron.*, vol. 49, DOI 10.1109/41.993270, no. 2, pp. 370–381, Apr. 2002.

[42] M. Apap, J. Clare, P. Wheeler, and K. Bradley, "Analysis and comparison of ac-ac matrix converter control strategies," *IEEE*

*34th Annual Conference on Power Electronics Specialist*, DOI 10.1109/PESC.2003.1216774, pp. 1287–1292, Jun. 2003.

[43] N. S. E. Malsch, "Recent advanced in the construction of polygonal finite element interpolants," *Arch. Computat. Methods Eng.*, vol. 11, DOI doi.org/10.1007/BF02905933, pp. 1–38, Sep. 2005.

[44] G. Dasgupta, "Interpolants within convex polygons: Wachspress shape functions," *Journal of Aerospace Engineering*, vol. 16, DOI doi.org/10.1061/(ASCE)0893-1321(2003)16:1(1), no. 1, Jan. 2003.

**Pawel Szczepankowski** (M'18) received his Ph.D. degree in electrical engineering in 2009 from the Gdansk University of Technology, Poland. He authored or co–authored more than 30 scientific and technical papers. His research interests include design, control, diagnostics, modeling and simulation of power electronic converters, including multilevel and matrix topologies, and signal processing with the use of advanced DSP and FPGA devices.

**Patrick Wheeler** (M'01–SM'10) received his B.Eng. (Hons.) degree in 1990 from the University of Bristol, UK. He received his PhD degree in Electrical Engineering for his work on Matrix Converters from the University of Bristol, UK in 1994. In 1993 he moved to the University of Nottingham and worked as a research assistant in the Department of Electrical and Electronic Engineering. In 1996 he became a Lecturer in the Power Electronics, Machines and Control Group at the University of Nottingham, UK. Since January 2008 he has been a Full Professor in the same research group. He was Head of the Department of Electrical and Electronic Engineering at the University of Nottingham from 2015 to 2018. He is currently the Head of the Power Electronics, Machines and Control Research Group, Global Direcotr of the University of Nottingham's Institute of Aerosapce Technology and is the Li Dak Sum Chair Professor in Electrical and Aerospace Engineering. He is a member of the IEEE PELs AdCom and was an IEEE PELs Distinguished Lecturer from 2013 to 2017. He has published 500 academic publications in leading international conferences and journals.

**Tomasz Bajdecki** received M.S. in electrical engineering from the Czestochowa University of Technology, Poland. in 1992. In 2003 he received a Ph.D. degree from Gdansk University of Technology for dissertation 'Control strategy for the matrix converter'. He is now with the Institute of Power Engineering, Gdansk, as a Research Staff Member. His main current interest is in the area of control of the high power converters.